APPLIED PHYSICS

Zero-energy bound states in the high-temperature superconductors at the two-dimensional limit

Chaofei Liu[1]*, Cheng Chen[1]*, Xiaoqiang Liu[1], Ziqiao Wang[1], Yi Liu[1], Shusen Ye[1], Ziqiang Wang[2], Jiangping Hu[3,4,5,6], Jian Wang[1,5,6,7]†

Majorana zero modes (MZMs) that obey the non-Abelian statistics have been intensively investigated for potential applications in topological quantum computing. The prevailing signals in tunneling experiments "fingerprinting" the existence of MZMs are the zero-energy bound states (ZEBSs). However, nearly all of the previously reported ZEBSs showing signatures of the MZMs are observed in difficult-to-fabricate heterostructures at very low temperatures and additionally require applied magnetic field. Here, by using in situ scanning tunneling spectroscopy, we detect the ZEBSs upon the interstitial Fe adatoms deposited on two different high-temperature superconducting one-unit-cell iron chalcogenides on $SrTiO_3$(001). The spectroscopic results resemble the phenomenological characteristics of the MZMs inside the vortex cores of topological superconductors. Our experimental findings may extend the MZM explorations in connate topological superconductors toward an applicable temperature regime and down to the two-dimensional (2D) limit.

INTRODUCTION

Quasi-particle excitations in superconductors crucially depend on impurity-scattering potentials, Cooper-pairing symmetry (*1*), and Andreev reflection processes (*2*). The zero-energy bound state (ZEBS) among them is particularly noteworthy, which can originate from the resonant tunneling involving topologically nontrivial Majorana zero mode (MZM) (*3*). Obeying the non-Abelian braiding statistics, the MZM is a promising building block for the fault-tolerant topological quantum computation (*4*). The theoretically predicted MZM platforms include Rashba two-dimensional (2D) semiconductors (*5*), semiconducting nanowires (*6*), spin-textured Fe atomic chains (*7*), and topological insulator ultrathin films (*8*) in proximity to Bardeen-Cooper-Schrieffer (BCS) superconductors. The ZEBSs proposed as the signatures of MZMs in these systems have been experimentally detected (*9*–*12*). However, the heterostructure-fabricating difficulty, the low experimental temperature (primarily ≤1.4 K), and the extra requirement of an applied magnetic field for those designs make the future applications of MZMs in quantum functionality electronics highly challenging.

The iron-based high-temperature superconductors provide alternative directions for pursuing the MZMs, where the topologically nontrivial phases have been theoretically predicted to universally exist (*13*–*17*). In recent experiments, the simultaneously discovered Dirac-type spin-helical surface state and s-wave superconducting (SC) gap in the iron chalcogenide material $FeTe_{0.55}Se_{0.45}$ highlight the existence of connate topological superconductivity at high temperatures (*18*). According to the Fu-Kane model, the proximitized interface between topological surface state (TSS) and s-wave pairing potential resembles a spinless $p_x + ip_y$ superconductor, which can host the MZMs in SC order parameter defects (*8*). Consistently, the ZEBSs bearing the characteristics of MZMs have been observed at the interstitial iron impurities and a fraction of magnetic vortices of bulk SC Fe(Te,Se) single crystals (*19*, *20*). Although bulk Fe(Te,Se) is a nominally perceived high-temperature superconductor, its SC transition temperature (T_c) is limited below 15 K (*19*). The relatively low T_c of Fe(Te,Se), together with the difficult-to-control character of magnetic field–induced vortices therein, poses barriers to technically realizing and freely manipulating the MZMs. It is accordingly desirable to investigate the Majorana physics both in higher T_c superconductors and under more feasibly manipulable physical settings.

The one-unit-cell (1-UC) FeSe (*21*) and Fe(Te,Se) (*22*) on $SrTiO_3$(001), showing enhanced high T_c typically above 60 K (*22*–*24*) and predicted to be topologically nontrivial (*15*, *17*), exemplify potential platforms to address those issues. Furthermore, although the magnetically ordered Yu-Shiba-Rusinov (YSR) (magnetic) chains placed on BCS superconductors have been systematically investigated in connection to MZMs (*7*), the individual YSR atom–based MZM configurations are scarcely proposed. Here, by in situ scanning tunneling spectroscopy (STS) (4.2 K unless specified; see Materials and Methods), we report the experimental discovery of the MZM-like ZEBSs induced by interstitial Fe adatoms on high-quality 1-UC FeSe and $FeTe_{0.5}Se_{0.5}$ on $SrTiO_3$(001) in the absence of external magnetic field. The spectroscopic results establish the generic existence of the ZEBSs in iron chalcogenide high-temperature superconductors at the 2D limit.

RESULTS AND DISCUSSION

Synthesis and multiband superconductivity of 1-UC FeSe

In the Brillouin zone (BZ) of 1-UC FeSe/$SrTiO_3$(001) (Fig. 1A), the Fermi surface consists of only electron pockets at the *M* points (Fig. 1, B and C) (*24*). By using the molecular beam epitaxy (MBE) technique, our 1-UC FeSe films were well prepared with atomically flat surfaces at both mesoscopic and microscopic scales (Fig. 1, D and E). As in previous reports (*21*, *24*), the tunneling spectrum (dI/dV versus V) measured on the 1-UC FeSe surface is fully gapped and typifies the multiband superconductivity as suggested by the high-resolution photoemission spectroscopy (Fig. 1F) (*25*). Along the trajectory in a single domain, the spatially resolved spectra repeatedly

[1]International Center for Quantum Materials, School of Physics, Peking University, Beijing 100871, China. [2]Department of Physics, Boston College, Chestnut Hill, MA 02467, USA. [3]Beijing National Laboratory for Condensed Matter Physics, and Institute of Physics, Chinese Academy of Sciences, Beijing 100190, China. [4]Kavli Institute of Theoretical Sciences, University of Chinese Academy of Sciences, Beijing 100190, China. [5]Collaborative Innovation Center of Quantum Matter, Beijing 100871, China. [6]CAS Center for Excellence in Topological Quantum Computation, University of Chinese Academy of Sciences, Beijing 100190, China. [7]Beijing Academy of Quantum Information Sciences, Beijing 100193, China.
*These authors contributed equally to this work.
†Corresponding author. Email: jianwangphysics@pku.edu.cn

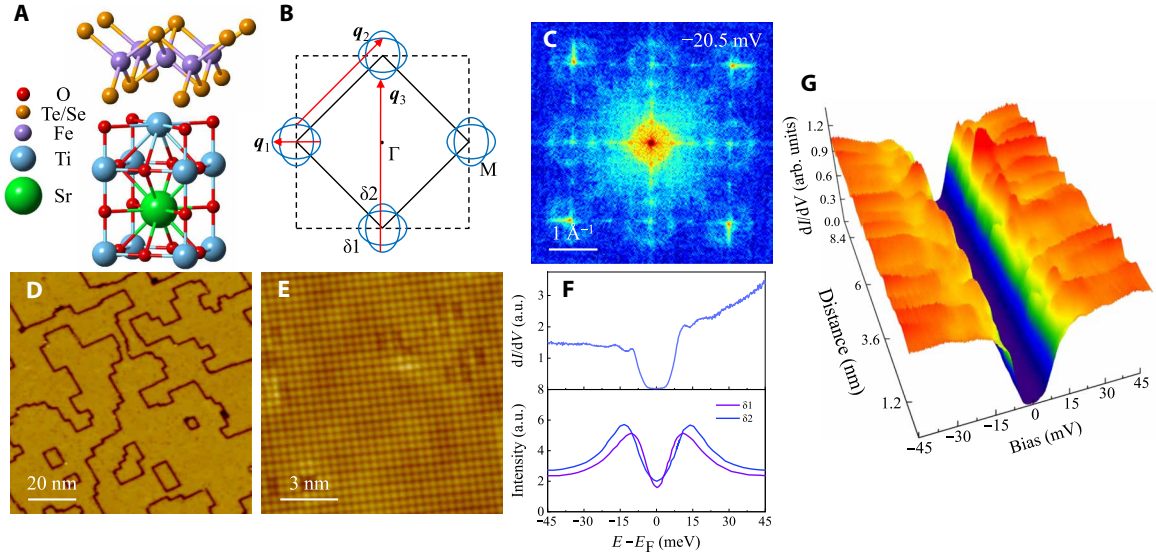

Fig. 1. Crystal structure, topographies, and multiband superconductivity of 1-UC FeSe/SrTiO$_3$(001). (**A**) Crystal structure and (**B**) Fermi surface topology in the folded BZ (solid black square) of 1-UC FeSe/SrTiO$_3$(001). $\boldsymbol{q}_1$, $\boldsymbol{q}_2$, and $\boldsymbol{q}_3$: Possible scattering vectors. (**C**) Fast Fourier transformation of the d*I*/d*V* mapping at −20.5 mV measured on the pristine 1-UC FeSe surface (28 nm × 28 nm; set point: $V = 0.06$ V, $I = 500$ pA; modulation: $V_{mod} = 1$ mV). Pocket-like scattering vectors can be seen and coincide with the hole pocket–absent Fermi surface topology in (B). (**D** and **E**) Topographic images of 1-UC FeSe film at different scales [100 nm × 100 nm (D) and 12.5 nm × 12.5 nm (E); set point: (D) $V = 0.6$ V, $I = 500$ pA; (E) $V = 0.2$ V, $I = 500$ pA]. (**F**) Comparison between tunneling spectrum (upper panel) and angle-resolved photoemission spectra (lower panel) (*25*) of 1-UC FeSe. The positions of δ1 and δ2 are marked in (B). (**G**) Spatially resolved tunneling spectra along a 9.4-nm trajectory. (F and G) Set point: $V = 0.04$ V, $I = 2500$ pA; modulation: $V_{mod} = 1$ mV (by default unless specified).

reveal the multiband pairing state with SC gaps near 9.5 and 16.0 meV, respectively (Fig. 1G). Therefore, a pristine high-temperature SC substrate [1-UC FeSe/SrTiO$_3$(001)] for the adsorbate deposition is well established.

Physical properties of detected ZEBS

The Fe atoms were deposited on the 1-UC FeSe surface at ~143 to 155 K at an ultralow coverage (section S1) for the formation of individual adatoms (Fig. 2A). In space, the Fe adatom locates above the energetically favorable, highly symmetric interstitial hollow site of four adjacent Se atoms (see also fig. S1A). Spectroscopically, the ZEBS modulated by adsorbate-substrate interaction (section S1) is induced by the interstitial Fe adatom, which appears as a zero-bias conductance peak (ZBCP) in the tunneling spectrum and is exceptionally sharp with a peak-to-dip d*I*/d*V* ratio of ~3 (Fig. 2B). Both the ultrahigh crystalline quality of 1-UC FeSe (Fig. 1, D and E) and the well-defined isolation of the adatom (Fig. 2A) exclude the extrinsic disorder effect on the detected ZBCP signal. Even sharper ZBCP line shape is expected when cooling down the experimental temperature (4.2 K) far below 1 K by a ^{3}He or a dilution refrigerator, which is beyond our current equipment capability and would stimulate further investigations in this direction. The magnetic impurity–induced ZEBS has been rarely reported in fully gapped superconductors (*19*) and constitutes the major finding in current study. Note also that the Fe adatom shows no sign of the ZEBS on ~30-UC FeSe/SiC(0001) (*26*). The contrast of the ZEBS that is present in 1-UC FeSe/SrTiO$_3$ and absent in ~30-UC FeSe/SiC, respectively, may signify the necessity of topologically nontrivial phases predicted only in the former (*17*) for the emergence of ZEBS.

To deeply reveal the ZEBS properties, the isolated interstitial Fe adatom was investigated in detail (Fig. 2, C to E). The spatial evolution of the tunneling spectra along a linecut departing from the adatom is presented in Fig. 2C. As moving away from the adatom center, the zero-bias signal drops abruptly but remains a single peak before becoming unidentifiable (see also fig. S2, A and B). The unsplitting behavior of the ZEBS here is noteworthy and reminiscent of the unsplit MZM-like ZEBS off magnetic vortex center in SC TSS (*20*). Moreover, the integrated low-bias density of states keeps roughly constant for the line spectra in Fig. 2C (fig. S2C), implying a spectral weight transfer from the coherence peaks to the ZBCP. To directly visualize the ZEBS distribution in space, a d*I*/d*V* mapping for the Fe-adatom topography in Fig. 2A was measured at 0 mV (Fig. 2D). Enhanced feature intimately bounded to the adatom edge was found in the ZEBS pattern, which correlates with the phase decoherence by the Fe adatom. For a more quantitative analysis, the linecut profiles starting from the adatom center were extracted from Fig. 2D and one of them, L, is exemplified in Fig. 2E. The exponential fitting of L yields a decay length, ξ, of 3.4 Å, which is nearly one order of magnitude smaller than the SC coherence length (2.45 nm) (*27*).

Scrutiny over nontopological physics

Kondo resonance (*28*) and impurity-scattering state (*1*) are available as the possible physical origins of the detected ZEBS, both of which can appear as single peaks around zero bias in the tunneling spectra. The Kondo effect originates from the exchange interaction between localized spins of magnetic impurities and conducting electrons in simple metals (Ag, Au, Cu, Pb, etc.). In experiments, the Kondo resonance is well described by a Fano line shape (*28*) and should deviate from zero energy due to finite potential scatterings in the SC state (*1*). Thus, the non-Fano–like (strikingly sharp) and precisely 0-mV conductance peak here is at odds with the Kondo scenario. To put further constraints on the interpretations of the detected ZEBS, the temperature-dependent experiment for the adatom-induced ZBCP was performed for 1-UC FeSe (Fig. 3A). As the temperature

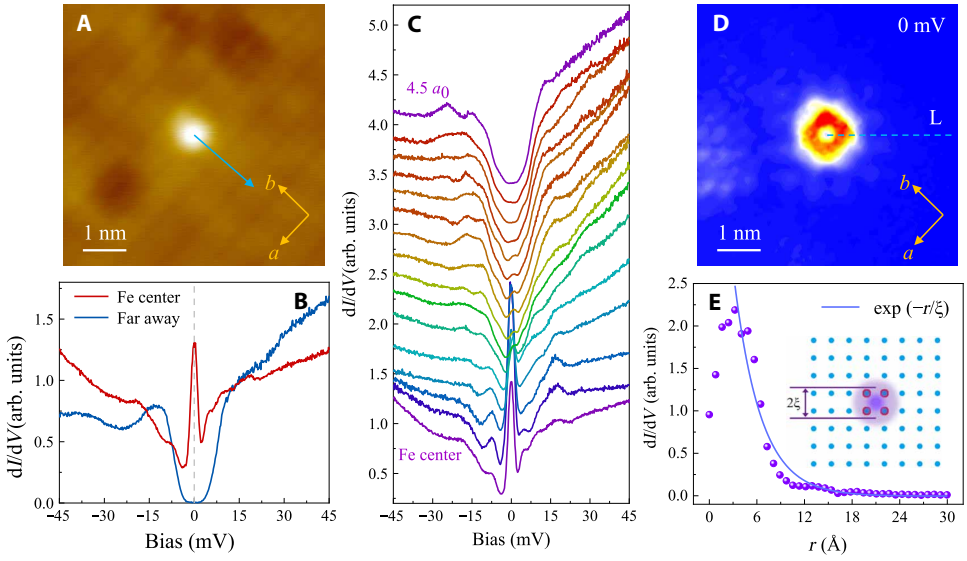

Fig. 2. Spatial evolution of the ZEBS in 1-UC FeSe. (**A**) Topographic image of an isolated Fe adatom (6 nm × 6 nm; set point: $V = 0.2$ V, $I = 500$ pA). (**B**) Tunneling spectra taken upon the Fe-adatom center and far away. (**C**) Spatially resolved tunneling spectra (vertically offset for clarity) along the arrow in (A). (**D**) dI/dV mapping at 0 mV for the Fe adatom in (A). (**E**) Linecut (solid symbols) along the dashed line, L, in (D) and corresponding exponential fitting (solid curve), showing ZBC as a function of the distance, r, relative to the Fe-adatom center. Fitting formula: dI/dV(r,0 mV) ∝ exp(− r/ξ); ξ: decay length. Inset: Schematic of the spatial distribution of Fe-adatom scattering.

increases, the peak intensity in the experimental spectrum decreases and completely merges into the background at 13 K well below T_c. Hence, the ZEBS is an emergent "sub-SC" phenomenon, where the nodeless SC gap away from the adatoms can be fully reserved (Fig. 2, B and C). If the ZEBS feature is dominated by the Kondo resonance, the ZBCP will be insensitive to superconductivity and will persist above T_c (*29*), which is evidently inconsistent with the observation here (Fig. 3A). On the other hand, being mutually correlated, the impurity state and the superconductivity should exhibit synchronized temperature dependence by the thermal broadening effect (*30*). The temperature evolution of the ZBCP with assumed impurity-state origin is obtained by convoluting the 4.2-K spectrum taken upon the Fe adatom by higher-temperature Fermi-Dirac distribution function (Fig. 3A). Apparently, the ZBCs (G_p) as a function of temperature for the experimental and convoluted ZEBS spectra substantially deviate from each other (Fig. 3B), quantitatively indicating that the conventional impurity-state explanation for the ZEBS is incompatible. Especially, in previous experimental studies, the near-zero-energy impurity states were mainly observed in d-wave superconductors at the strong scattering (unitary) limit (*1*). Besides the non–d-wave [e.g., extended $s_{\pm}$-wave (*31*)] pairing possibility of the 1-UC FeSe/$SrTiO_3$(001), the scattering from the Fe adatom inducing the ZEBS here is not at the unitary limit in statistics (section S1).

Recent theoretical advances have extended the magnetic impurity states to iron-based superconductors treated as spin-singlet pairing with both sign-preserving (s_{++}-wave) and sign-reversing ($s_{\pm}$-wave; nodal and nodeless d-wave) SC-gap functions over the Fermi surfaces (*32*–*34*). In these models, the impurity-state energy can be tuned to zero for a critical strength of the scattering potential (*32*, *34*), which appears in agreement with the detected ZEBS and demands more experiments to scrutinize the ZEBS identity. Physically, the impurity state is doubly degenerate at zero energy with both spin-up and spin-down components (*29*), which will be split by an applied magnetic field. This is analogous to the theoretical prediction that the quantum mechanically coupled magnetic adatom dimer will hybridize and split the degenerate impurity state into bonding and antibonding counterparts (*35*), where one adatom is effectively situated in the magnetic exchange field of the other. The unavailability of external magnetic field in our apparatus motivates us to alternatively study the ZEBS response in the adatom dimer. Surprisingly, the ZEBS remains a robust single peak at zero energy for two closely located interstitial Fe adatoms on 1-UC FeSe (Fig. 3, D and E). The presence of spin-orbit coupling (SOC) has been shown to suppress the Zeeman field–induced splitting of the ZEBSs localized at magnetic impurities for bulk Fe(Te,Se) with electron and hole Fermi surface nesting and $s_{\pm}$-type pairing (*36*). Whether this theoretical conclusion is valid remains to be examined for the Fe-adatom dimer in 1-UC FeSe, where the hole Fermi pocket is absent. All these aforementioned results for the detected ZEBS in 1-UC FeSe are poorly reconciled within the conventional impurity-state framework.

Possibility of MZM

The inconsistency between ZBCP and nontopological interpretations raises the concern whether a topologically nontrivial picture is responsible for the ZEBS emergence. The 2D superconductors with Rashba SOC can turn into the topological SC (TSC) states via sufficiently strong time reversal symmetry–breaking Zeeman field, where the MZMs emerge as the ZEBSs in magnetic vortex cores. Equivalently, the exchange field from generic magnetic impurities can serve in place of the Zeeman coupling to break the time reversal symmetry. The physical properties of the magnetic impurity–induced YSR states in this type of topological superconductors and superfluids, including bound-state spectra, band structures, wave functions, and spatial profiles of SC order parameters, have been extensively investigated and found intriguingly different from those in nontopological cases (*37*–*39*). Recently, the quantum anomalous vortices (QAVs) were theoretically proposed to be generated by interstitial magnetic transition metal ions in a strongly spin-orbit–coupled s-wave superconductor in the absence of external magnetic field (*40*). When superconductivity is coupled to the spin-helical Dirac fermion TSS,

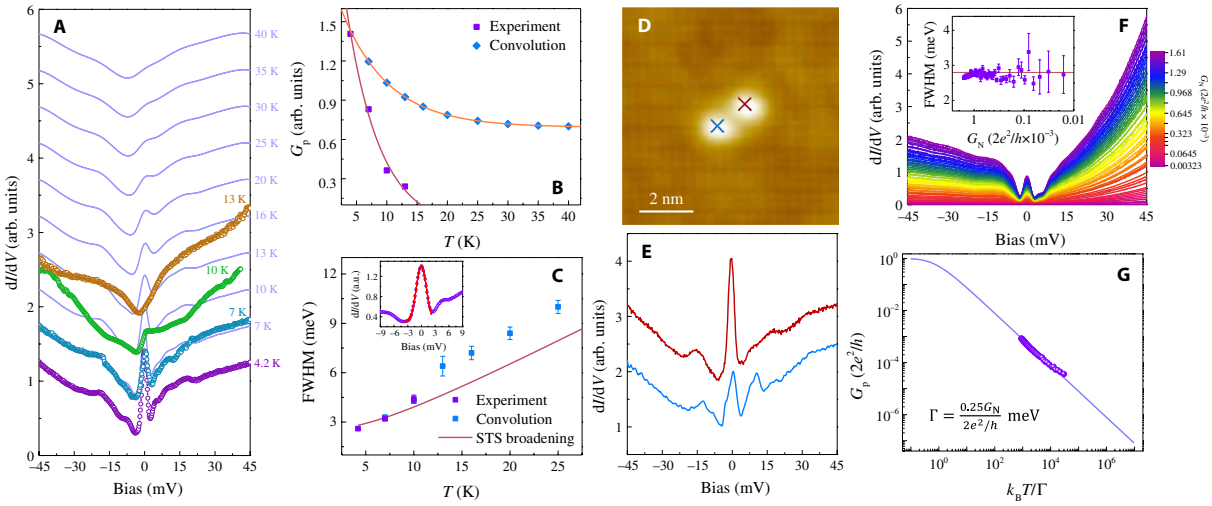

Fig. 3. Perturbation of the ZEBS in 1-UC FeSe by temperature, a neighboring Fe adatom, and different tunneling barriers. (**A**) Temperature dependence of the experimental tunneling spectra (open symbols) measured upon the Fe-adatom center in Fig. 2A and the convoluted 4.2-K spectra (solid curves) by Fermi-Dirac distribution function at higher temperatures (both vertically offset for clarity). (**B**) ZBC, G_p, plotted as a function of temperature (solid symbols) extracted from (A). (**C**) FWHM of the ZBCP (solid symbols) in the experimental and convoluted spectra of (A). The solid curve is the spectral energy resolution combining both instrumental and thermal broadening, $\Delta E = \sqrt{(2.5eV_{mod})^2 + (3.5k_BT)^2}$. Inset: Exemplifying the Gaussian fitting to the ZBCP, which defines the FWHM and error bars standard deviations adopted throughout. (**D**) Topographic image of an Fe-adatom dimer (8 nm × 8 nm; set point: $V = 0.1$ V, $I = 500$ pA). (**E**) Tunneling spectra (vertically offset for clarity) taken upon the Fe adatoms in (D). (**F**) Tunneling barrier conductance G_N dependence of the ZEBS spectra (4.2 K), where G_N is parameterized as the tunneling conductance ($G_N = I/V$). Inset: FWHM of the ZBCP in the main-panel spectra under different G_N. The solid curve is ΔE at 4.2 K. (**G**) Scaling analysis of G_p of the tunneling spectra of (F). Solid curve, calculated G_p for the MZM at different k_BT/Γ according to Eq. 1; solid symbols, experimental G_p plotted as a function of G_N rescaled as k_BT/Γ to match the calculated curve, yielding $\Gamma = \frac{0.25G_N}{2e^2/h}$meV.

the magnetic ion–trapped QAV supports the MZM in the core, which follows the same spirit of the Fu-Kane model (*8*) but without requiring the external field. There is surely no TSS available in connate 1-UC FeSe. However, if the 2D SC state contains the necessary ingredients for being topologically nontrivial, then the nucleation of the QAV at the interstitial Fe-adatom site is likely to induce a ZEBS-typified MZM. On the basis of the observation of Fermi level–crossed linearly dispersive bands, the undoped parent phase of 1-UC FeSe/$SrTiO_3$ was demonstrated to be Dirac semimetallic in nature by photoemission spectroscopy (*41*), which can be induced by the substrate tensile strain field and SOC (*16*). When electron doping is introduced, an odd-parity TSC state was theoretically conjectured to emerge in the nodeless s-wave pairing channel (*17*). While much work is needed to explore the topological properties of the SC state in 1-UC FeSe, these recent developments, together with the detected ZEBS and its incompatibility especially with the conventional impurity-scattering state, suggest the QAV to be a possible candidate for the ZEBS physics. We are thus motivated to further investigate the characteristics of the ZBCP in 1-UC FeSe and compare them with those of the MZM that behaves as the ZEBS within the topologically nontrivial scenario.

Phenomenologically, the ZBCP "melting" temperature (T_c^{ZBCP}) in nearly all literature reporting the MZM-like signatures (*9*, *10*, *20*, *42*) is far below the T_c of the pristine SC components in corresponding MZM configurations. This empirical relation, $T_c^{ZBCP} \ll T_c$, is well satisfied in the present 1-UC FeSe situation (i.e., ~13 K ≪ ~60 K), implying the likelihood of Majorana signal involved in the Fe adatom–induced ZEBS. By comparing with the impurity state–like convoluted spectra in Fig. 3A, where the ZBCP persists up to ≥35 K, we conclude that the disappearance of the experimental ZBCP above 13 K is not a simple consequence of thermal broadening. Thus, additional T_c^{ZBCP} suppression mechanism must exist, which can be described by the Majorana "poisoning" through thermally excited quasi-particles (*43*).

The full width at half maximum (FWHM) of the MZM peak in the tunneling spectrum is determined by instrumental, thermal, and tunneling broadening (*44*). To quantitatively test the MZM explanation for the ZEBS, the FWHM of the ZBCP in the experimental and convoluted spectra at various temperatures (Fig. 3A) was extracted and shown in Fig. 3C. The spectrum broadening, ΔE, combining both instrumental and thermal effects is also plotted for comparison. It is seen that the FWHM of the ZBCP is limited by ΔE for the experimental ZEBS spectra, falling within the MZM picture, but exceeds ΔE for the convoluted ZEBS spectra for temperature ≥ 13 K. Moreover, as shown in Fig. 3F, the experimental ZEBS at 4.2 K exists robustly and the ZBCP FWHM remains approximately ΔE-limited across nearly three orders of magnitude in the tunneling barrier conductance G_N. The fact that the experimental ZEBS is mainly spectrum-broadened by ΔE indicates a negligible tunneling coupling strength (Γ) and especially coincides with the spectral expectation for the Majorana ZBCP with an intrinsically single-peak nature. The latter excludes the possibilities of both impurity state–related multifold degeneracy at zero energy and densely packed low-energy quasi-particle excitations around the Fermi level. The fact that only the ZEBS exists within the SC gap is consistent with the expulsion of nonzero-energy Caroli–de Gennes–Martricon (CdGM) vortex core states beyond the SC gap in the QAV theory, protecting the MZM by preventing the mixing with topologically trivial higher-level CdGMs (*40*).

Dictated by particle-hole symmetry, the incoming electron and reflected hole in the tunneling process into an MZM via resonant Andreev reflection equally contribute to the zero-energy tunneling amplitude, resulting in the quantized ZBC of $2e^2/h$ at zero temperature

(*3*). Because of the small tunneling coupling strength Γ and the Majorana poisoning by nontopological quasi-particles, the ZBC quantization is extremely challenging to achieve in STS experiments. Nevertheless, because of the universal scaling function obeyed by Majorana ZBCP (*45*), the ZBCs below the conductance-quantization region can be used to trace down the zero-temperature limit as a consistency check of the ZEBS nature. Specifically, at weak-tunneling ($\Gamma \ll \Delta_{1,2}$) and low-temperature ($k_BT \ll \Delta_{1,2}$; k_B, Boltzmann constant) conditions, the ZBC of tunneling-broadened finite-temperature MZM spectrum in subgap regime, G_p, is given by

$$G_p = \frac{2e^2}{h}\int_{-\infty}^{\infty} \frac{\Gamma^2}{E^2+\Gamma^2}\frac{1}{4k_BT\cosh^2(E/2k_BT)}\,dE \quad (1)$$

which only depends on the dimensionless ratio, k_BT/Γ. In accordance with the spinless model for MZM tunneling, $\Gamma = \eta\frac{G_N}{2e^2/h}$ for sufficiently small $\frac{G_N}{2e^2/h}$ (*44*), corresponding to the situation in STS configurations. The G_N-dependent G_p extracted from Fig. 3F for 1-UC FeSe can be rescaled as a function of k_BT/Γ at different values of η, which is found to collapse onto the scaling curve (Eq. 1) for η = 0.25 (Fig. 3G). The yielded $\Gamma = \frac{0.25G_N}{2e^2/h}$ meV for our experimental G_N range is ~4 to 6 orders of magnitude smaller than the instrumental and thermal spectrum broadening, Δ*E*. The vanishingly small Γ is reasonably consistent with the weak-tunneling condition as concluded from the ZEBS spectrum width analysis and naturally explains the weak G_N dependence of ZBCP FWHM (Fig. 3F). All above experimental observations resemble phenomenologically the spectroscopic signatures of the MZM. Pushing the experimental data [$G_p(G_N)$] toward the asymptotic small k_BT/Γ limit at ultralow temperatures and ultrahigh tunneling conductance will unveil more solid evidence for the MZM in future investigations.

Reproducibility of ZEBS in 1-UC $FeTe_{0.5}Se_{0.5}$

The sharply defined ZBCP induced by the interstitial Fe adatom was reproduced in a different 2D iron chalcogenide high-temperature superconductor, 1-UC $FeTe_{1-x}Se_x$ ($x \approx 0.5$) (Fig. 4, A and B). The preparation of high-quality 1-UC Fe(Te,Se) film showing high T_c is exceedingly challenging experimentally, and the in situ STS studies have been rarely reported. By using the MBE technique (see Materials and Methods), we successfully grew the highly disorder-free 1-UC $FeTe_{0.5}Se_{0.5}$ on $SrTiO_3$(001) with both mesoscopic and microscopic atomic flatness. The nominal composition of 1-UC $FeTe_{0.5}Se_{0.5}$ was calculated by measuring the thickness of the 2nd-UC Fe(Te,Se) film and independently counting the ratio of Se/Te. Both methods yield consistent stoichiometry of 1-UC Fe(Te,Se). As observed in 1-UC FeSe, the ZEBS in 1-UC $FeTe_{0.5}Se_{0.5}$ induced by the interstitial Fe adatom maintains an unsplit ZBCP spectrum that fades out spatially away from the adatom (Fig. 4C) and is intimately localized by the adatom (Fig. 4D) with a decay length of ~6.4 Å (Fig. 4E).

The spectroscopic characteristics of the ZEBS in 1-UC FeSe are all highly reproducible in 1-UC $FeTe_{0.5}Se_{0.5}$ (Fig. 5). Compared to 1-UC FeSe, the ZBCP in the experimental spectrum of 1-UC $FeTe_{0.5}Se_{0.5}$ disappears at a higher temperature of 20 K, which is still well below T_c, in contrast to the thermally convoluted ZEBS spectrum with assumed impurity-state origin (Fig. 5, A and B). For an Fe-adatom dimer, the ZEBS spectrum remains singly peaked (Fig. 5, D and E). Both the premature thermal melting and the spectral unsplitting against local magnetic exchange field for the detected ZEBS in 1-UC $FeTe_{0.5}Se_{0.5}$ reemphasize the difficulty in describing the ZEBS in terms of the conventional impurity-scattering state. Furthermore, the FWHM result is consistent with the intrinsically single-peak nature of the detected ZBCP (Fig. 5C), as expected for the MZM. Most intriguingly, the experimentally detected ZEBS (4.2 K) exhibits rather robust existence for a wide range of the tunneling barrier conductance G_N over several orders of magnitude (Fig. 5F). By detailed scaling analysis based on Eq. 1, the G_N-dependent G_p extracted from the experimental ZEBS spectra in Fig. 5F is quantitatively described by the universal scaling of Majorana ZBCP (Fig. 5G), yielding η = 0.35, comparable with that (0.25) obtained in 1-UC FeSe.

By first-principles calculations, $FeTe_{1-x}Se_x$ ($x = 0.5$) has been predicted to show the nontrivial topology characterized by an odd Z_2 invariant (*14*), which can survive down to the 1-UC limit for $x < 0.7$ (*15*). Therefore, the epitaxially prepared 1-UC $FeTe_{0.5}Se_{0.5}$ is situated in the predicted topological regime of both bulk and ultrathin $FeTe_{1-x}Se_x$. It is truly remarkable that the robust MZM-like ZEBSs persist at the interstitial Fe-adatom sites in the 1-UC $FeTe_{0.5}Se_{0.5}$, as shown by our experiments. The reproducibility of the phenomenological MZM features in different 1-UC iron chalcogenides possibly suggests a common topologically nontrivial origin of the detected ZEBSs. Notably, free-standing 1-UC FeSe, the $x = 1$ limit of 1-UC $FeTe_{1-x}Se_x$, appears topologically trivial by first-principles calculations (*15*). Nevertheless, to simulate the substrate effect, more realistic calculations of 1-UC FeSe by adopting the measured lattice constant [3.82 Å (*23*)] yield topologically nontrivial, band-inverted electronic structures (*15*). The result reconciles the topological phases predicted by including the contribution of substrate effect directly in the full model Hamiltonian (*16*).

SUMMARY AND PERSPECTIVES

In summary, we have reported the observation of the ZEBSs manifested as the ZBCPs in STS upon the interstitial Fe adatoms on two different 2D high-temperature superconductors, 1-UC FeSe and $FeTe_{0.5}Se_{0.5}$. All the presented data are highly similar for these two compounds, both demonstrating the inadequacy of the ZEBS interpretation based on Kondo resonance and conventional impurity state. More detailed experiments of the ZEBSs show overall consistency with the MZM phenomenology, including their temperature and tunnel barrier conductance dependences. The analyses of ZBCP FWHM and tunneling coupling suggest the spectroscopic absence of other adatom-induced bound states, possibly expelled outside the SC gap due to the exchange field of the Fe adatoms. This situation is analogous to the theoretical proposal of the QAVs nucleated at the magnetic ions in superconductors with strong SOC, where the exchange field leads to the expulsion of the CdGM vortex core states beyond the SC-gap energy (*40*). In light of the possible topological phases (*15*–*17*, *41*) and SOC-induced spin-triplet pairing components in 1-UC FeSe and Fe(Te,Se), the hidden mechanism responsible for the observed ZEBSs may be the QAVs nucleated at the magnetic Fe adatoms in 2D topological superconductors. Different from the Fu-Kane model (*8*), within the QAV scenario for the MZMs in the ultra-2D 1-UC FeSe and $FeTe_{0.5}Se_{0.5}$ in the absence of external magnetic field, the magnetic flux lines produced by and connecting the quantum anomalous vortex-antivortex pairs are expected to form closed loops around the 1-UC SC layer (*40*).

Other possibilities for the ZEBS emergence include the existence of helical topological mirror superconductivity (*38*), odd-frequency

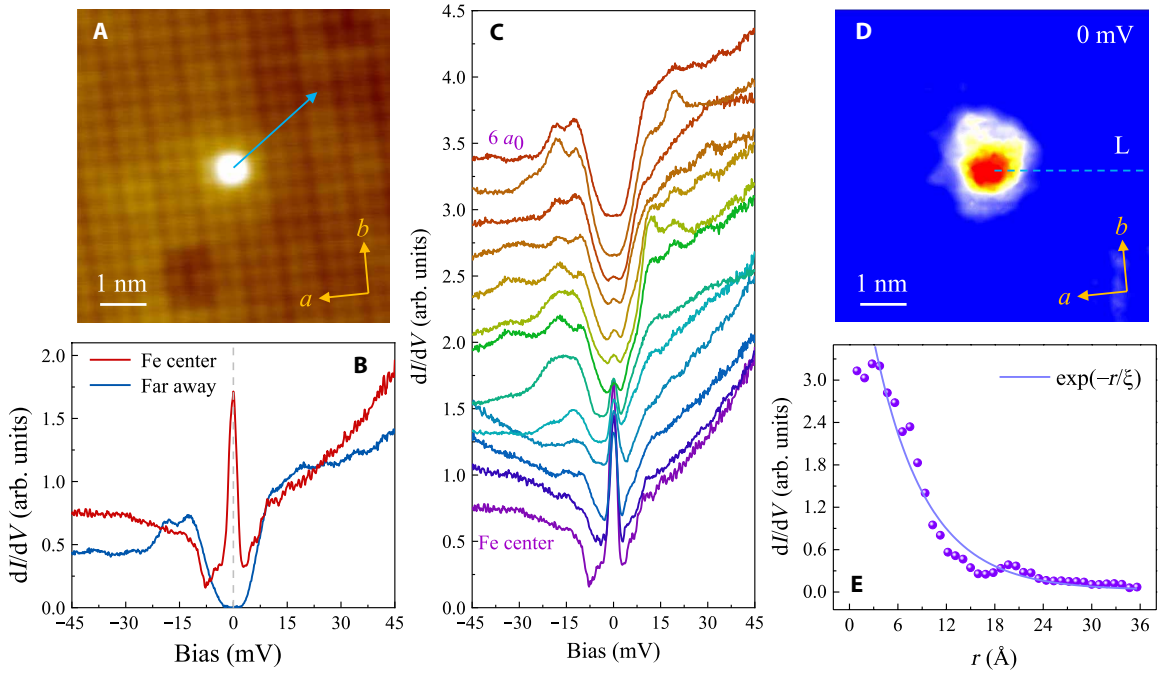

Fig. 4. Spatial evolution of the ZEBS in high-quality 1-UC $FeTe_{0.5}Se_{0.5}/SrTiO_3$(001). (**A**) Topographic image of an isolated Fe adatom (6.75 nm × 6.75 nm; set point: $V = 0.1$ V, $I = 500$ pA). (**B**) Tunneling spectra taken upon the Fe-adatom center and far away. (**C**) Spatially resolved tunneling spectra (vertically offset for clarity) along the arrow in (A). (**D**) dI/dV mapping at 0 mV for the Fe adatom in (A). (**E**) Linecut (solid symbols) along the dashed line, L, in (D) and corresponding exponential fitting (solid curve) by dI/d$V(r,0\ \text{mV}) \propto \exp(-r/\xi)$, showing ZBC as a function of the distance, r, relative to the Fe-adatom center.

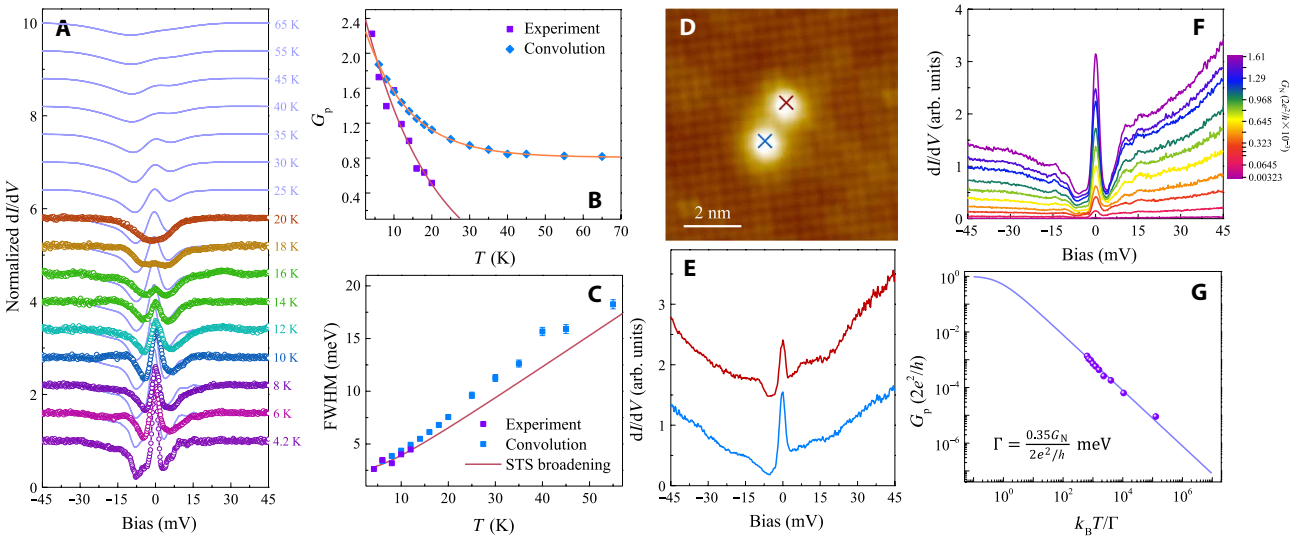

Fig. 5. Perturbation of the ZEBS in 1-UC $FeTe_{0.5}Se_{0.5}$ by temperature, a neighboring Fe adatom, and different tunneling barriers. (**A**) Temperature dependence of the experimental tunneling spectra (open symbols) measured upon the Fe-adatom center in Fig. 4A and the convoluted 4.2-K spectra (solid curves) by Fermi-Dirac distribution function at higher temperatures (both vertically offset for clarity). The experimental spectra have been normalized by their respective cubic-polynomial backgrounds for clarity, which are obtained from fitting to the spectra for bias $|V| \geq 30$ mV. (**B**) G_p plotted as a function of temperature (solid symbols) extracted from (A). (**C**) FWHM of the ZBCP (solid symbols) in the experimental and convoluted spectra of (A). The solid curve is the spectral energy resolution combining both instrumental and thermal broadening ΔE plotted versus temperature. (**D**) Topographic image of an Fe-adatom dimer (8 nm × 8 nm; set point: $V = 0.1$ V, $I = 500$ pA). (**E**) Tunneling spectra (vertically offset for clarity) taken upon the Fe adatoms in (D). (**F**) G_N dependence of the ZEBS spectra (4.2 K). (**G**) Scaling analysis of G_p of the tunneling spectra of (F). Solid curve, calculated G_p for the MZM at different k_BT/Γ according to Eq. 1; solid symbols, experimental G_p plotted as a function of G_N rescaled as k_BT/Γ to match the calculated curve, yielding $\Gamma = \frac{0.35G_N}{2e^2/h}$ meV.

pairing state (*46*), d + *i*d–wave superconductivity (*47*), and the potentially modulated magnetic skyrmion (*48*) preluded by Fe adatom–reconstructed electronic structures (section S3). We emphasize that the observed ZEBSs in truly high-temperature superconductors at the 2D limit are unidentified previously and existing theories cannot provide a precise and direct explanation at the present

time. Here, we have discussed just a few possibilities and hope our findings will stimulate further theoretical and experimental investigations. A thorough understanding of the observed ZEBSs would require detailed knowledge of the interplay among adsorbate-substrate interaction, local magnetic structure, SOC, and superconductivity.

Compared to bulk Fe(Te,Se) studied in (*19*, *20*), the high T_c of 1-UC FeSe and $FeTe_{0.5}Se_{0.5}$ substantially increases T_c^{ZBCP} (section S4), which is an essential step toward the commercially available liquid-nitrogen temperature regime. Particularly, the rigorous two-dimensionality of 1-UC FeSe and $FeTe_{0.5}Se_{0.5}$ calls for a fundamentally different mechanism of the potential MZM in 1-UC iron chalcogenides from that proposed for bulk Fe(Te,Se), which relies on the TSSs created through the out-of-plane band inversion (*14*). In addition, the 1-UC iron chalcogenides adsorbed by interstitial Fe adatoms also offer overwhelming advantages for studying the ZEBS in the following aspects: (i) The MBE technique used for FeSe and $FeTe_{0.5}Se_{0.5}$ growth guarantees the highly disorder-free sample quality; (ii) the comparatively large SC gaps for 1-UC FeSe and $FeTe_{0.5}Se_{0.5}$ protect the ZEBS against perturbations; and (iii) for future applications, the experimental systems described here integrate nearly all the desired ingredients for feasibly realizing and manipulating the MZM-like ZEBS: The unnecessity of external magnetic field for inducing the ZEBS, the ultrashort ZEBS decay length, and the technically feasible scanning tunneling microscope (STM) manipulation of adatoms further push our experimental systems toward applicable quantum functionality electronics (section S4).

MATERIALS AND METHODS

Sample growth and tunneling experiments

The experiments were conducted in an ultrahigh-vacuum (~2×10^{-10} mbar) MBE-STM combined system (Scienta Omicron). The 0.7% w.t. Nb-doped $SrTiO_3$(001) was thermally boiled by 90°C deionized water for 50 min and chemically etched by 12% HCl solution for 45 min (*21*). Then, the $SrTiO_3$ was loaded into the MBE chamber and pretreated by the Se-flux method (*21*). The 1-UC FeSe ($FeTe_{0.5}Se_{0.5}$) film was grown by coevaporating high-purity Fe (99.994%) and Se (99.999%) [Se (99.999%) and Te (99.999%)] from an e-beam evaporator and Knudsen cell(s), respectively, with the $SrTiO_3$ held at 400°C (340°C), followed by annealing at 450°C (380°C) for 3 hours. The Fe adatoms were deposited on 1-UC FeSe and $FeTe_{0.5}Se_{0.5}$ surfaces in the MBE chamber nominally at ~143 to 155 K. After annealing and depositing procedures, the 1-UC FeSe and $FeTe_{0.5}Se_{0.5}$ films were transferred in situ to STM chamber for topography and spectroscopy imaging. A polycrystalline PtIr tip was used throughout the experiments. The topographic images were obtained in a constant-current mode. The tunneling spectra were acquired by using the standard lock-in technique with a bias modulation typically of 1 mV at 1.7759 kHz. Radio-frequency noise filters were used to enhance the signal-to-noise ratio. Both topography and spectroscopy were measured with a bias voltage equivalently applied to the sample at 4.2 K unless specified. All the topographic images were post-processed by the SPIP software.

Theoretical calculations for Fe adatom/1-UC FeSe

First-principles calculations were carried out using the Vienna Ab initio simulation package (VASP) with Perdew-Burke-Ernzerhof functional. The local density approximation (LDA) + U method with effective U = 0.4 eV on Fe atom was adopted to properly represent the local electronic correlations. The plane-wave cutoff energy was fixed to 400 eV, and the crystal structures were relaxed until the atomic forces were smaller than 0.01 eV/Å. A k-point mesh of $9 \times 9 \times 1$ centered at Γ point was used in the calculation of single-layer FeSe unit cell. A checkerboard antiferromagnetic spin configuration was adopted. To simulate the Fe adatom, a supercell of $5 \times 5 \times 1$ was constructed. SOC was included for all calculations.

SUPPLEMENTARY MATERIALS

Supplementary material for this article is available at http://advances.sciencemag.org/cgi/content/full/6/13/eaax7547/DC1

Section S1. Adsorbate-substrate interaction–modulated ZEBS
Section S2. Additional data of the spatially evolving ZEBS
Section S3. Fe adatom–reconstructed electronic structures
Section S4. Prospects for the local ZEBS detection in connate high-temperature superconductors
Fig. S1. Statistically correlated bound-state energy and Fe adatom height for 1-UC FeSe.
Fig. S2. More analyses of the spatially evolving ZEBS in Fig. 2C.
Fig. S3. A $5 \times 5 \times 1$ supercell of 1-UC FeSe with Fe adatom (blue) in the center.
Fig. S4. Electronic structures of 1-UC FeSe reconstructed by Fe adatom.
Fig. S5. Histogram of the ZEBS-related parameters in different configurations plotted for direct comparison.
Table S1. Summary of the ZEBS-related information in literature.
Reference (*49*)

REFERENCES AND NOTES

1. A. V. Balatsky, I. Vekhter, J.-X. Zhu, Impurity-induced states in conventional and unconventional superconductors. *Rev. Mod. Phys.* **78**, 373–433 (2006).
2. C. W. J. Beenakker, *Colloquium*: Andreev reflection and Klein tunneling in graphene. *Rev. Mod. Phys.* **80**, 1337–1354 (2008).
3. K. T. Law, P. A. Lee, T. K. Ng, Majorana fermion induced resonant Andreev reflection. *Phys. Rev. Lett.* **103**, 237001 (2009).
4. C. Nayak, S. H. Simon, A. Stern, M. Freedman, S. Das Sarma, Non-Abelian anyons and topological quantum computation. *Rev. Mod. Phys.* **80**, 1083–1159 (2008).
5. J. D. Sau, R. M. Lutchyn, S. Tewari, S. Das Sarma, Generic new platform for topological quantum computation using semiconductor heterostructures. *Phys. Rev. Lett.* **104**, 040502 (2010).
6. R. M. Lutchyn, J. D. Sau, S. Das Sarma, Majorana fermions and a topological phase transition in semiconductor-superconductor heterostructures. *Phys. Rev. Lett.* **105**, 077001 (2010).
7. S. Nadj-Perge, I. K. Drozdov, B. A. Bernevig, A. Yazdani, Proposal for realizing Majorana fermions in chains of magnetic atoms on a superconductor. *Phys. Rev. B* **88**, 020407 (2013).
8. L. Fu, C. L. Kane, Superconducting proximity effect and Majorana fermions at the surface of a topological insulator. *Phys. Rev. Lett.* **100**, 096407 (2008).
9. V. Mourik, K. Zuo, S. M. Frolov, S. R. Plissard, E. P. A. M. Bakkers, L. P. Kouwenhoven, Signatures of Majorana fermions in hybrid superconductor-semiconductor nanowire devices. *Science* **336**, 1003–1007 (2012).
10. H. Zhang, C.-X. Liu, S. Gazibegovic, D. Xu, J. A. Logan, G. Wang, N. van Loo, J. D. S. Bommer, M. W. A. de Moor, D. Car, R. L. M. Op Het Veld, P. J. van Veldhoven, S. Koelling, M. A. Verheijen, M. Pendharkar, D. J. Pennachio, B. Shojaei, J. S. Lee, C. J. Palmstrom, E. Bakkers, S. D. Sarma, L. P. Kouwenhoven, Quantized Majorana conductance. *Nature* **556**, 74–79 (2018).
11. S. Nadj-Perge, I. K. Drozdov, J. Li, H. Chen, S. Jeon, J. Seo, A. H. MacDonald, B. A. Bernevig, A. Yazdani, Observation of Majorana fermions in ferromagnetic atomic chains on a superconductor. *Science* **346**, 602–607 (2014).
12. H.-H. Sun, K.-W. Zhang, L.-H. Hu, C. Li, G.-Y. Wang, H.-Y. Ma, Z.-A. Xu, C.-L. Gao, D.-D. Guan, Y.-Y. Li, C. Liu, D. Qian, Y. Zhou, L. Fu, S.-C. Li, F.-C. Zhang, J.-F. Jia, Majorana zero mode detected with spin selective Andreev reflection in the vortex of a topological superconductor. *Phys. Rev. Lett.* **116**, 257003 (2016).
13. X. Wu, S. Qin, Y. Liang, C. Le, H. Fan, J. Hu, $CaFeAs_2$: A staggered intercalation of quantum spin Hall and high-temperature superconductivity. *Phys. Rev. B* **91**, 081111 (2015).
14. Z. Wang, P. Zhang, G. Xu, L. K. Zeng, H. Miao, X. Xu, T. Qian, H. Weng, P. Richard, A. V. Fedorov, H. Ding, X. Dai, Z. Fang, Topological nature of the $FeSe_{0.5}Te_{0.5}$ superconductor. *Phys. Rev. B* **92**, 115119 (2015).
15. X. Wu, S. Qin, Y. Liang, H. Fan, J. Hu, Topological characters in $Fe(Te_{1-x}Se_x)$ thin films. *Phys. Rev. B* **93**, 115129 (2016).
16. N. Hao, J. Hu, Topological phases in the single-layer FeSe. *Phys. Rev. X* **4**, 031053 (2014).
17. N. Hao, S.-Q. Shen, Topological superconducting states in monolayer $FeSe/SrTiO_3$. *Phys. Rev. B* **92**, 165104 (2015).

18. P. Zhang, K. Yaji, T. Hashimoto, Y. Ota, T. Kondo, K. Okazaki, Z. Wang, J. Wen, G. D. Gu, H. Ding, S. Shin, Observation of topological superconductivity on the surface of an iron-based superconductor. *Science* **360**, 182–186 (2018).
19. J.-X. Yin, Z. Wu, J.-H. Wang, Z.-Y. Ye, J. Gong, X.-Y. Hou, L. Shan, A. Li, X.-J. Liang, X.-X. Wu, J. Li, C.-S. Ting, Z.-Q. Wang, J.-P. Hu, P.-H. Hor, H. Ding, S. H. Pan, Observation of a robust zero-energy bound state in iron-based superconductor Fe(Te,Se). *Nat. Phys.* **11**, 543–546 (2015).
20. D. Wang, L. Kong, P. Fan, H. Chen, S. Zhu, W. Liu, L. Cao, Y. Sun, S. Du, J. Schneeloch, R. Zhong, G. Gu, L. Fu, H. Ding, H.-J. Gao, Evidence for Majorana bound states in an iron-based superconductor. *Science* **362**, 333–335 (2018).
21. Q.-Y. Wang, Z. Li, W.-H. Zhang, Z.-C. Zhang, J.-S. Zhang, W. Li, H. Ding, Y.-B. Ou, P. Deng, K. Chang, J. Wen, C.-L. Song, K. He, J.-F. Jia, S.-H. Ji, Y.-Y. Wang, L.-L. Wang, X. Chen, X.-C. Ma, Q.-K. Xue, Interface-induced high-temperature superconductivity in single unit-cell FeSe films on $SrTiO_3$. *Chin. Phys. Lett.* **29**, 037402 (2012).
22. F. Li, H. Ding, C. Tang, J. Peng, Q. Zhang, W. Zhang, G. Zhou, D. Zhang, C.-L. Song, K. He, S. Ji, X. Chen, L. Gu, L. Wang, X.-C. Ma, Q.-K. Xue, Interface-enhanced high-temperature superconductivity in single-unit-cell $FeTe_{1-x}Se_x$ films on $SrTiO_3$. *Phys. Rev. B* **91**, 220503 (2015).
23. W.-H. Zhang, Y. Sun, J.-S. Zhang, F.-S. Li, M.-H. Guo, Y.-F. Zhao, H.-M. Zhang, J.-P. Peng, Y. Xing, H.-C. Wang, T. Fujita, A. Hirata, Z. Li, H. Ding, C.-J. Tang, M. Wang, Q.-Y. Wang, K. He, S.-H. Ji, X. Chen, J.-F. Wang, Z.-C. Xia, L. Li, Y.-Y. Wang, J. Wang, L.-L. Wang, M.-W. Chen, Q.-K. Xue, X.-C. Ma, Direct observation of high-temperature superconductivity in one-unit-cell FeSe films. *Chin. Phys. Lett.* **31**, 017401 (2014).
24. Z. Wang, C. Liu, Y. Liu, J. Wang, High-temperature superconductivity in one-unit-cell FeSe films. *J. Phys. Condens. Matter* **29**, 153001 (2017).
25. Y. Zhang, J. J. Lee, R. G. Moore, W. Li, M. Yi, M. Hashimoto, D. H. Lu, T. P. Devereaux, D.-H. Lee, Z.-X. Shen, Superconducting gap anisotropy in monolayer FeSe thin film. *Phys. Rev. Lett.* **117**, 117001 (2016).
26. C.-L. Song, Y.-L. Wang, P. Cheng, Y.-P. Jiang, W. Li, T. Zhang, Z. Li, K. He, L. Wang, J.-F. Jia, H.-H. Hung, C. Wu, X. Ma, X. Chen, Q.-K. Xue, Direct observation of nodes and twofold symmetry in FeSe superconductor. *Science* **332**, 1410–1413 (2011).
27. Q. Fan, W. H. Zhang, X. Liu, Y. J. Yan, M. Q. Ren, R. Peng, H. C. Xu, B. P. Xie, J. P. Hu, T. Zhang, D. L. Feng, Plain *s*-wave superconductivity in single-layer FeSe on $SrTiO_3$ probed by scanning tunnelling microscopy. *Nat. Phys.* **11**, 946–952 (2015).
28. V. Madhavan, W. Chen, T. Jamneala, M. F. Crommie, N. S. Wingreen, Tunneling into a single magnetic atom: Spectroscopic evidence of the Kondo resonance. *Science* **280**, 567–569 (1998).
29. K. J. Franke, G. Schulze, J. I. Pascual, Competition of superconducting phenomena and Kondo screening at the nanoscale. *Science* **332**, 940–944 (2011).
30. K. Hirata, K. Yamamoto, K. Iijima, J. Takada, T. Terashima, Y. Bando, H. Mazaki, Tunneling measurements on superconductor/insulator/superconductor junctions using single-crystal $YBa_2Cu_3O_{7-x}$ thin films. *Appl. Phys. Lett.* **56**, 683–685 (1990).
31. M. Khodas, A. V. Chubukov, Interpocket pairing and gap symmetry in Fe-based superconductors with only electron pockets. *Phys. Rev. Lett.* **108**, 247003 (2012).
32. W.-F. Tsai, Y.-Y. Zhang, C. Fang, J. Hu, Impurity-induced bound states in iron-based superconductors with *s*-wave $\cos k_x \cdot \cos k_y$ pairing symmetry. *Phys. Rev. B* **80**, 064513 (2009).
33. A. Akbari, I. Eremin, P. Thalmeier, Magnetic impurity resonance states and symmetry of the superconducting order parameter in iron-based superconductors. *Phys. Rev. B* **81**, 014524 (2010).
34. S. Mukherjee, M. N. Gastiasoro, B. M. Andersen, Impurity-induced subgap bound states in alkali-doped iron chalcogenide superconductors. *Phys. Rev. B* **88**, 134508 (2013).
35. M. E. Flatté, D. E. Reynolds, Local spectrum of a superconductor as a probe of interactions between magnetic impurities. *Phys. Rev. B* **61**, 14810 (2000).
36. K. Seo, J. D. Sau, S. Tewari, Effects of spin-orbit coupling on zero-energy bound states localized at magnetic impurities in multiband superconductors. *Phys. Rev. B* **95**, 205107 (2017).
37. Y. Kim, J. Zhang, E. Rossi, R. M. Lutchyn, Impurity-induced bound states in superconductors with spin-orbit coupling. *Phys. Rev. Lett.* **114**, 236804 (2015).
38. Y.-Y. Tai, H. Choi, T. Ahmed, C. S. Ting, J.-X. Zhu, Edge states and local electronic structure around an adsorbed impurity in a topological superconductor. *Phys. Rev. B* **92**, 174514 (2015).
39. H. Hu, L. Jiang, H. Pu, Y. Chen, X.-J. Liu, Universal impurity-induced bound state in topological superfluids. *Phys. Rev. Lett.* **110**, 020401 (2013).
40. K. Jiang, X. Dai, Z. Wang, Quantum anomalous vortex and Majorana zero mode in iron-based superconductor Fe(Te,Se). *Phys. Rev. X* **9**, 011033 (2019).
41. S. Kanayama, K. Nakayama, G. N. Phan, M. Kuno, K. Sugawara, T. Takahashi, T. Sato, Two-dimensional Dirac semimetal phase in undoped one-monolayer FeSe film. *Phys. Rev. B* **96**, 220509 (2017).
42. S. Sasaki, M. Kriener, K. Segawa, K. Yada, Y. Tanaka, M. Sato, Y. Ando, Topological superconductivity in $Cu_xBi_2Se_3$. *Phys. Rev. Lett.* **107**, 217001 (2011).
43. J. R. Colbert, P. A. Lee, Proposal to measure the quasiparticle poisoning time of Majorana bound states. *Phys. Rev. B* **89**, 140505 (2014).
44. F. Setiawan, C.-X. Liu, J. D. Sau, S. Das Sarma, Electron temperature and tunnel coupling dependence of zero-bias and almost-zero-bias conductance peaks in Majorana nanowires. *Phys. Rev. B* **96**, 184520 (2017).
45. F. Nichele, A. C. C. Drachmann, A. M. Whiticar, E. C. T. O'Farrell, H. J. Suominen, A. Fornieri, T. Wang, G. C. Gardner, C. Thomas, A. T. Hatke, P. Krogstrup, M. J. Manfra, K. Flensberg, C. M. Marcus, Scaling of Majorana zero-bias conductance peaks. *Phys. Rev. Lett.* **119**, 136803 (2017).
46. Y. Tanaka, M. Sato, N. Nagaosa, Symmetry and topology in superconductors—Odd-frequency pairing and edge states. *J. Phys. Soc. Jpn.* **81**, 011013 (2012).
47. M. Sato, Y. Takahashi, S. Fujimoto, Non-Abelian topological orders and Majorana fermions in spin-singlet superconductors. *Phys. Rev. B* **82**, 134521 (2010).
48. G. Yang, P. Stano, J. Klinovaja, D. Loss, Majorana bound states in magnetic skyrmions. *Phys. Rev. B* **93**, 224505 (2016).
49. H. Wang, H. Wang, H. Liu, H. Lu, W. Yang, S. Jia, X.-J. Liu, X. C. Xie, J. Wei, J. Wang, Observation of superconductivity induced by a point contact on 3D Dirac semimetal Cd_3As_2 crystals. *Nat. Mater.* **15**, 38–42 (2016).

Acknowledgments: We thank J. Feng, X. C. Xie, and Q.-H. Wang for helpful discussions. **Funding:** This work was financially supported by the National Natural Science Foundation of China (nos.11888101 and 11774008), National Key R&D Program of China (nos. 2018YFA0305604 and 2017YFA0303302), Strategic Priority Research Program of Chinese Academy of Sciences (no. XDB28000000), Beijing Natural Science Foundation (no. Z180010), and U.S. Department of Energy, Basic Energy Sciences (no. DE-FG02-99ER45747). **Author contributions:** J.W. conceived and instructed the research. C.L. and C.C. prepared the samples. C.L., C.C., Ziqiao Wang, and Y.L. carried out the STS experiments. X.L. performed the first-principles calculations. C.L., C.C., and S.Y. analyzed the data. C.L., Ziqiang Wang, J.H., and J.W. wrote the manuscript with input from all authors. **Competing interests:** The authors declare that they have no competing interests. **Data and materials availability:** All data needed to evaluate the conclusions in the paper are present in the paper and/or the Supplementary Materials. Additional data related to this paper may be requested from the authors.

Submitted 19 April 2019
Accepted 6 January 2020
Published 25 March 2020
10.1126/sciadv.aax7547

Citation: C. Liu, C. Chen, X. Liu, Z. Wang, Y. Liu, S. Ye, Z. Wang, J. Hu, J. Wang, Zero-energy bound states in the high-temperature superconductors at the two-dimensional limit. *Sci. Adv.* **6**, eaax7547 (2020).